INTERNATIONAL ATOMIC ENERGY AGENCY
UNITED NATIONS EDUCATIONAL, SCIENTIFIC AND CULTURAL ORGANIZATION
INTERNATIONAL CENTRE FOR THEORETICAL PHYSICS
I.C.T.P., P.O. BOX 586, 34100 TRIESTE, ITALY, CABLE: CENTRATOM TRIESTE

H4.SMR/642 - 18

College on Methods and Experimental Techniques in Biophysics

28 September - 23 October 1992

The Liquid and Solid Phases of Water:
an Extensive Molecular Dynamic Simulation with the Ab-Initio NCC Potential

E. CLEMENTI

CRS4, Cagliari, Italy

THE LIQUID AND SOLID PHASES OF WATER: AN EXTENSIVE MOLECULAR DYNAMIC SIMULATION WITH THE AB-INITIO NCC POTENTIAL

Enrico Clementi, Giorgina Corongiu and Francesco Sciortino

CRS4, Centro di Ricerca, Sviluppo e Studi Superiori in Sardegna

P.O. Box 488, 09100 Cagliari Italy

Abstract

We present results on the reliability of the ab-initio, polarizable and flexible NCC-vib potential [1,2] in describing the structure and the dynamics of the liquid and solid phases of water. For both structural and dynamic quantities the agreement between experimental and numerical results is good. A "substance" very similar to the "real water" has been indeed created on the basis of ab-inito quantum mechanical calculations. This gives confidence to use the simulations to examine features that are not directly measurable, but of central importance for the understanding of the water structure and dynamics.

Introduction: In the last few years many new potentials have been proposed to model water-water interactions. The availability of computers with large memory and fast processing units has made possible to step from the early two body description of molecular interactions toward more complex many body descriptions. This is particularly relevant in the case of assemblies of water molecules, where polarization contributions make up a significant part of the total binding energy.

The new many-body potentials should be suitable to describe successfully all phases of water: the gas phase, the liquid phase and the many forms of ice. Indeed, one of the major goal of these potentials should be to give the possibility to study phase transitions, inter-phases, water close to biomolecules, etc., within a unifying framework, i.e. ***without to chose an ad hoc potential for each specific application.***

In literature, two classes of many body potentials have been developed to describe the water-water interactions: (i) the class of empirical potentials, where the parameters in the analytic form of the potential energy are parametrized against experimental data, and (ii) the class of ab-initio potentials, where the parameters

are determined on the base of quantum mechanical calculations on small clusters of water molecules.

In this paper we review the existing numerical simulation based on the ab-initio polarizable potential which has been developed by Nieser, Corongiu and Clementi (NCC in the following) [1]. Many parts of this article follow the original papers [2-4], to which we refer the interested reader for further informations. The good agreement between the experimental and simulated data found in both phases for static and dynamics properties suggests that a computer "substance" very similar to real water, *based only on ab-inito quantum mechanical calculations*, has indeed been created.

1. The NCC potential: The NCC potential has been parametrized against quantum mechanical calculations at the MP4 level for water dimers and at the HF level for water trimers [1]. It is composed by two contributions: a two body potential, $V_{two-body}$, and a polarization term, E_{pol}. The polarization effects in the NCC potential are represented by a point polarizability along the two OH bonds. An intramolecular term, V_{intra}, has been recently added to the NCC potential to take into account the intramolecular degrees of freedom. The potential is therefore composed by three terms:

$$V_{NCC} = V_{2-body} + V_{pol} + V_{intra} \tag{1}$$

where the V_{2-body} is an additive term, which takes care of the repulsion between atoms and of their electrostatic interactions; V_{pol} is a polarization term expressed as

$$V_{pol} = -\frac{1}{2}\sum_{i}^{N_m}\sum_{\lambda}^{N_d}\vec{\mu}_{i\lambda}^{ind}\vec{E}_{i\lambda}^{q} \tag{2}$$

where $\vec{E}_{i\lambda}^{q}$ is the electric field generated by the charges q on molecule i at the λ position, N_m the number of molecules in the system, N_d the number of induced dipole moments on one molecule, $\vec{\mu}_{i\lambda}$, given by

$$\vec{\mu}_{i\lambda}^{ind} = \hat{\alpha}_{i\lambda}[\vec{E}_{i\lambda}^{q} + \sum_{k\neq i}^{N_m}\sum_{\nu}^{N_d}\hat{T}_{i\lambda k\nu}\vec{\mu}_{k\nu}^{ind}] \tag{3}$$

with $\hat{T}$ the dipole-dipole matrix and $\hat{\alpha}_{i\lambda}$ the polarizabily tensor.

The intra-molecular potential, V_{intra}, is also derived from *ab initio* computations [5]. It is expressed, up to quartic terms, in function of the three internal coordinates of the water molecule, the changes in the OH bond lengths and in the OHO bond angle. The equilibrium bond length and bond angle predicted by the potential, for one water molecule in the gas phase, are 0.9576 $\AA$ and 104.59° respectively, to be compared with the experimental values [6] of 0.9572 $\AA$ and 104.5°.

2. Computational Details: Simulations in the liquid phase have been performed with samples of 512 water molecules at several temperatures, and at a density of 0.997 gr/cm^3. Simulations in the solid phase (ice I_h) have been performed with 432 molecules [4]. The simulations have been carried out at constant energy and constant density (NVE ensemble). Periodic boundaries conditions have been applied to simulate the infinite system. To handle the electrostatic interactions we have used the Reaction Field technique in the liquid phase and the Ewald summation in the solid phase. The self-consistent set of induced dipole moments was calculated by an iterative method, as explained in detail in Ref. [1]. A sixth-order Gear predictor corrector method was used to integrate the equations of motion with a time step of 0.125 femto seconds. We refer to the original papers for further informations.

3. The Liquid Phase: Static and Dynamic Properties. To stress the reliability of our interaction potential we start comparing (Fig. 1A) the experimental x-ray intensity data [7a] at T=298 K with the same quantity calculated from the MD simulated data at T=305 K. Notice the overall satisfactory agreement between simulated and experimental data, the best thus far reported including even those based on interaction potentials fitted to experimental data. Characteristic quantities in the x-ray scattering are the position and intensity of the first two peaks, which are known to vary drastically with temperature [7]. The position of the first and second structural peaks in $S(k)$ as a function of temperature, for both experimental [7b] and simulated data are reported in Fig. 1-B.

We notice that, for temperatures above the supercooled region, both, the intensity (not reported) and the position of the first peak grow almost linearly with temperature, whereas there is a decrease for the second peak; eventually at higher temperatures than those here considered, the two peaks merge into a single one.

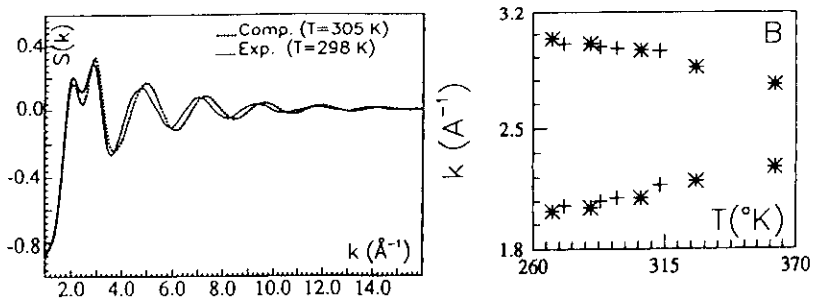

Fig. 1: A) X-ray scattering intensity: Comparison between simulated and experimental data. B) Temperature dependence of the the first two peeks in S(k). (+) experiments (Ref. 7b), (*) simulations (Ref. 3).

Again, the NCC data agree well, qualitatively and quantitatively, with the experimental results.

As for the X-ray data, we find a quantitative agreement also for neutron diffraction data (Fig. 2-A). The position of first peak in the structure factor measured by neutrons decreases on cooling the sample as shown in Fig. 2-B and approaches the value characteristic of the amorphous low density ice. For a more detailed comparison see Ref. 3.

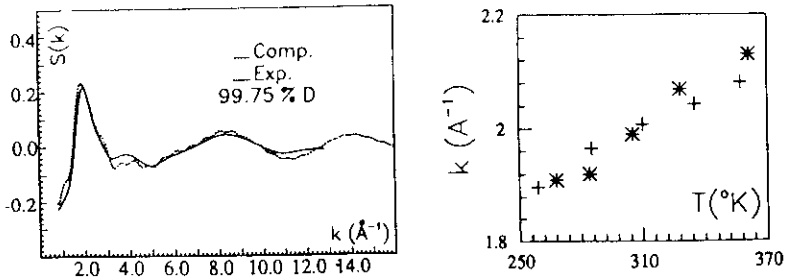

Fig. 2: (A) Comparison between the experimental and the computed neutron structure factor. (B) Temperature dependence of the position of the first peek in the neutron S(k); (+) experiments (Ref. 7b), (*) simulations (Ref. 3).

The data shown agree qualitatively and quantitatively with the experimental results. Thus, we are encouraged to use the simulations to examine the simulated partial radial distribution functions in deep detail, even if a clear comparison with

experiments can not be performed. Indeed, to extract partial radial distribution functions from neutron scattering experiments one has to join data from mixture with different water/deuterium content. This introduces a certain amount of ambiguity due to the different structures of liquid light water and liquid heavy water.

In Fig. 3 we compare the simulated oxygen-oxygen pair correlation function, g_{OO} and g_{OH}, data with those obtained from x-ray and neutron diffraction experiments by Narten [7,8] and from neutron diffraction by Soper [9], both at a temperature of 298K. There are notable differences in the two experimental sets of data. The MD data agree very well with Soper's data.

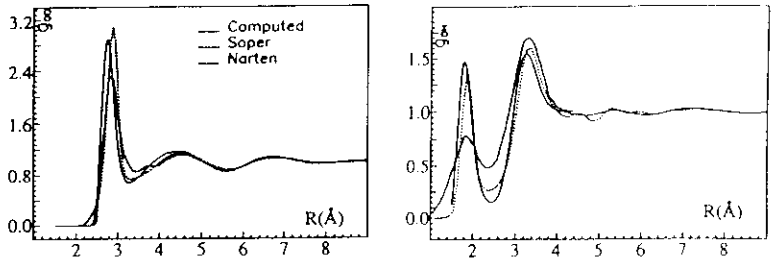

Fig. 3: Oxygen-Oxygen (left) and Oxygen-Hydrogen (right) radial distribution functions. Comparison between simulated and experimental data.

The $g_{OO}(r)$ at four different temperatures are reported in Fig. 4. We note the existence of radial positions [10] where the value of the radial distribution function does not change. Indeed, as shown in Fig. 5-A the difference between any couple of temperatures is zero exactly at the same points. This property was observed experimentally by Bosio et al. (Fig. 5-B). Bosio, Chen and Teixeira [7b, 11] made accurate measurements of the oxygen radial distribution function for two different temperatures T_1 and T_2 chosen such that the density ρ of water is the same for both temperatures; this is possible due to the existence of a maximum in the function $\rho(T)$. By subtracting the respective radial distribution functions, they obtained *isochoric temperature differential functions* displaying the remarkable property that only the heights of the peaks and valleys (but not their positions) depend on temperature.

The existence of point invariant for a change in temperature is also found in the integral of the radial distribution function, i.e. in the number of neighbour found inside a sphere centered on a selected atom (Fig. 4-B). The properties of invariance

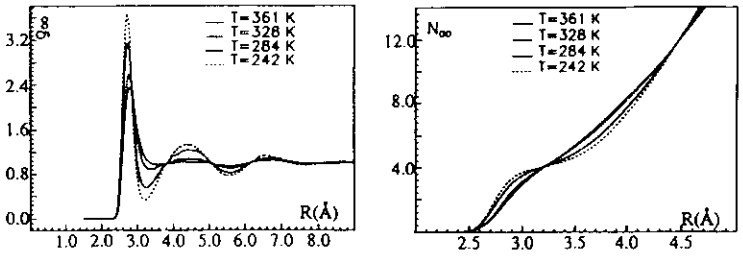

Fig. 4: A) Oxygen-Oxygen radial distribution function. Temperature dependence. B) Coordination numbers, $N_{OO}(r,T)$, at different temperatures

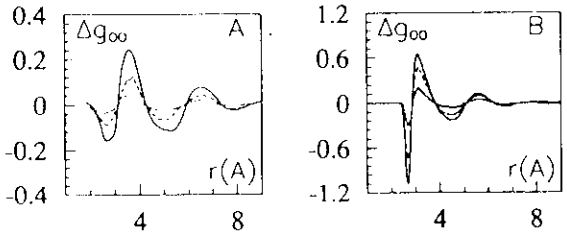

Fig. 5: A) $\Delta g_{OO}(r,\Delta T)$ from MD simulation. $\Delta T = 77,56$ and $33°K$ B) $\Delta g_{OO}(r,\Delta T)$ from experiments. $\Delta T = 55,23.7$ and $22.6°K$ (Ref. 11).

shown by the $g(r)$ and its integral speak strongly in favour of a decomposition of the local environment in two large groups.

If we assume [12], as a first approximation, that in the liquid there are two species A and B, with *temperature-dependent* concentrations $x_A(T)$ and $x_B(T)$ and with $(x_A + x_B = 1)$, then the total radial distribution function g_T is related to the radial distribution functions g_A and g_B of species A and B by the relation

$$g_T(r,T) = x_A(T)g_A(r) + x_B(T)g_B(r). \qquad (4)$$

With this functional choice, the points were $g_A(r) = g_B(r)$ are temperature invariant. The fortuitous crossing of the different temperature is ruled out by the existence of more than one invariant point, not only in $g(r)$ but also in the integral of $g(r)$, up to about 7 Å. From Eq. 4 we have indeed

$$N_{OO}(r) = \int g_T(r,T)r^2dr = x_A(T)\int g_A(r)r^2dr + x_B(T)\int g_B(r)r^2dr \qquad (5)$$

In the same way the isochoric temperature differential function is given by

$$g_T(r,T_2) - g_T(r,T_1) = [x_B(T_2) - x_B(T_1)][g_B(r) - g_A(r)]. \qquad (6)$$

By using Eq. (6), we can interpret the change shown in Fig. 5 on increasing the $T_2 - T_1$ range as an effect of the decreasing concentration of the B species on cooling.

It is important to stress that the two species, A and B, are characterized by a variety of geometries whose probability distribution is expressed by $g_A(r)$ and $g_B(r)$. Also, being the liquid a mixture of A and B, one would expect a cross term in the expression for the radial distribution function (Eq. 4). The fact that this term is not needed for distances shorter than 7 Å, suggests that the local structure imposed by the central molecule extends up to that distance.

From the number of molecules within a radius r equal to the first minimum in the g_{OO} as a function of temperature we can get informations on the properties of the molecules belonging to group A (dominant at low T) and to group B. We find that type A molecules are surrounded in average by 4 neighbours while the type B molecules by five or more neighbours. From the shape of the $N_{OO}(r)$ curves we also see that the low temperature species is characterized by a non-homogeneous "local" density (structured liquid), which becomes more and more homogeneous on increasing the temperature. The presence of more than four neighbour is sometimes interpreted to mean that the tetrahedral network cannot be perfect but must contain defects of some sort. The presence of these defects (caused by "extra molecules" in the first coordination shell) is potentially of considerable importance to the *dynamic* properties of water [13,14]. It has been argued that the presence of a fifth molecule acts as 'catalyst' for the restructuring of the HB network even though the thermal energy kT is much smaller than the HB energy [13,14].

An extensive analysis of dynamical properties in the liquid phase can be found in Ref. 15. Here we focus only on the low frequency part of the density of states.

The density of states (DOS), a measure of the number of modes at frequency ω available to the atoms in the system, can be obtained from the Fourier transform of the atoms velocity autocorrelation function. In the hindered translations region the density of states of the proton and oxygen atoms coincides, being the excitations

related to the translational motion of the center of mass. This fact, along with the large incoherent scattering length of the protons, enables the experimental measure of an effective DOS in the translation region for light water.

Fig.6 shows the $DOS(\omega)$. We observe a broad band extending from 0 to about 300 cm^{-1} with a first peak at about 60 cm^{-1} and a second one at about 170 cm^{-1} (easily obtainable by deconvolution). These two bands result mostly from the oxygen atom trajectories since the oxygen atom motions are very close to the center of mass of a water molecule. From the figure we see a temperature effect, specifically a shift towards lower frequencies by increasing the temperature. Therefore, the motions are becoming more and more free, the higher the temperature. The first peak has been associated to the oxygen-oxygen-oxygen bending and the second one to the oxygen-oxygen stretching, namely intermolecular motions relating oxygen atoms. (O-H...O).

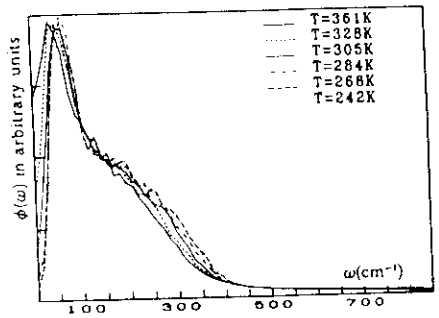

Fig. 6: Translational bands. Oxygen power spectrum at the indicated temperatures.

The data of Fig. 6 clearly shows two regions separated by an isosbestic point at about 130 cm^{-1}. Our data nicely agree with the experimental data of Ref. 16, where a detailed analysis is reported for liquid water in the temperature range 276-368 K. In the quoted paper, it is found that the first band covers two different modes; one at 50 cm^{-1} moves towards lower frequencies as temperature increases, while a second one, which occurs at 70 cm^{-1}, moves instead in the opposite direction, as temperature increases. From Fig. 6 we can not distinguish the two bands, but, since the first peak is broad, definitely can accommodate more than one component. Work is in progress to assess the presence or not of two different modes in the frequency

range 0-100 and to elucidate if this is due to bifurcated hydrogen bonds as proposed in Ref. 16.

4. The I_h Solid Phase: Static and Dynamic Properties. A full account on the static properties of the simulated solid phase of water can be found in Ref. 4. Here we show only the intermolecular OO radial distribution functions ($g(r)$). The $g(r)$ calculated for the Ice I_h structure at T=100 K is drawn as full line. The broken line shows the $g(r)$ function calculated for the same system after an energy minimization (T=0 K). We observe that the disorder connected with the proton positions affects significantly also the oxygen positions and broadens the distribution for intermolecular OO distance. We find that the first neighbors OO distance at T=0 K (i.e. when only positional disordered is taken into account) has a spread of 0.02 $\AA$. The estimated value for the same quantity from the refined neutron data is a few hundredth of an angstrom [17].

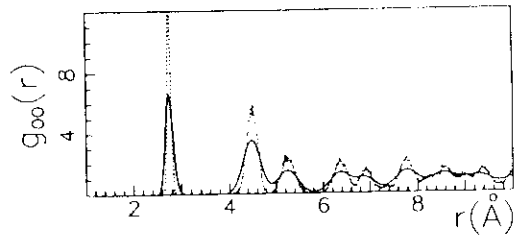

Fig. 7: Oxygen-Oxygen radial distribution function. T=100 K (full line) and T=0 K (dashed line).

Fig. 8-A shows, for the region 0-300 cm^{-1} the calculated DOS in I_h and the inelastic incoherent neutron experimental results from Ref. [18].

Our simulation results show several peaks, which correspond to the acoustic and optical modes of the crystal. We observe that the NCC-vib DOS very well reproduces the regions below 100 and above 150 cm^{-1}, but fails to reproduce the correct position of the peaks in the region between 100 and 150 cm^{-1}.

We have calculated the dispersion relations along three directions in $\vec{k}$ space, (0001), $(11\bar{2}0)$, $(01\bar{1}0)$, which correspond in real space to the c-axis direction and to two directions perpendicular to the c-axis. On the hexagonal lattice the directions $(11\bar{2}0)$, $(01\bar{1}0)$ correspond to the two lines connecting first and second neighbors,

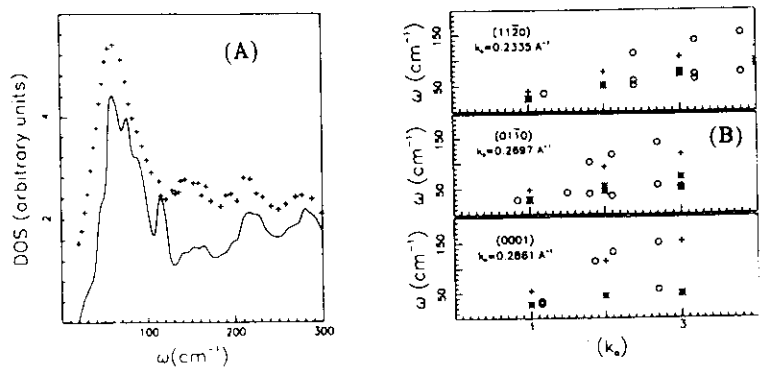

Fig. 8: A) Deuterium atom density of states for Ice I_h (full line) compared with the low frequency incoherent inelastic neutron scattering data of Ref. [17] (+). The simulated data have been scaled in the frequency axis by 1.054 to take into account the different molecular mass of H_2O (used in the experiments) compared to D_2O (used in the simulation). B) Dispersion relations for the longitudinal (+) and transverse (*) acoustic modes in the (0001), (11$\bar{2}$0), (01$\bar{1}$0) directions. Note that the crystallographic point K coincides with $k = 4k_o$ in the (11$\bar{2}$0) direction, the point M with $k = 3k_o$ in the (01$\bar{1}$0) direction, and the point A with $k = 1.5k_o$ in the (0001). The calculated frequencies are compared with the coherent inelastic neutron scattering data (o) of Ref. 19. The k_o value for each direction is also shown in the figure.

respectively. The crystal symmetries allow us to average $J_{\vec{k}}(\omega)$ with respect to $\vec{k}$ vectors with the same magnitude. The dispersion relationships for the three studied directions are shown in Fig. 8-B. Also reported in Fig. 8-B are the corresponding experimental points from Ref. [19]. The corresponding acoustic velocities, obtained as the ratio of frequency and wave vector for the smallest $\vec{k}$ value available for each direction, are respectively 2.1, 2.1 and 2.0 km/s for the transverse modes and 3.3, 3.4 and 3.8 km/s for the longitudinal modes to be compared with the experimental values for polycrystalline ice I_h of 2.0 and 3.9 km/s [20].

The agreement between simulated and experimental data is very good in the (0001) direction (c-axis) and for the transverse phonons in the (11$\bar{2}$0) and (01$\bar{1}$0) directions. Less satisfactory are the results for the acoustic longitudinal phonons whose values at the zone boundary are in general 10-20 % smaller than the corresponding experimental data. We interpret the disagreement between computed and

experimental DOS in the 100-140 cm^{-1} region as originating from the error in the acoustic longitudinal phonons frequencies. Thus, there is space for further improvement in the more sensitive region of the potential hyper surface that controls the acoustic longitudinal phonons.

Recently we have also calculated the Raman and Infrared spectra for our NCC-vib simulation [21]. These spectra have been calculated by using experimental values for the molecular polarizability, hyper-polarizability and dipole-quadrupole polarizability in conjunction with values for the n-pole propagator evaluated from the trajectories obtained from molecular dynamics (MD) simulations. We have found that the Raman and IR spectra in ice in the region 0-400 cm^{-1} are dominated by the collision induced terms. As previously found for liquid water [22], Raman and IR spectra of the solid phase are related to the phonons not through modulation of the molecular polarizability but through modulation of the intermolecular distances. We refer the interest reader to Ref. 21.

5. Conclusions. The NCC-vib interaction potential has been obtained by fitting ab initio data rather than experimental data. This potential represents the latest evolution which started with a Hartree-Fock potential [23] and later has been refined with others, including the MCY [24]. As it is known, this evolution is due both to increased performance in computational means and advances in the theoretical development.

The agreement between experimental data and simulation data obtained for NCC-vib is good both for single particle properties as well as collective properties. The same potential is able to describe with the same accuracy both the liquid and the solid phase in a wide range of temperatures. The absence of any "ad hoc" parametrization in the derivation of the potential makes the agreement in the collective behavior remarkable.

The capability of the NCC potential of reproducing closely many experimental quantities gives confidence to use the simulations to examine features that are not directly measurable, but of central importance for the understanding of water structure and dynamics. We have presented here one example of such investigations: the study of the temperature evolution of the radial distribution function in terms of a

progressive increase on cooling of the fraction of tetrahedrally coordinated molecules. Further examples can be found in Ref. 15 where the network topology is studied and in Ref. 21 where the separation of the Raman spectra in its constituent contributions is performed. We stress that computer simulations, once validated by the comparison with the experimental quantities, become very powerful as techniques of analysis. The noise level can be controlled since related to the available computer time. In addition, the availability of trajectories produced by MD simulations enables to perform, in a simple way, checks on the approximations involved in the calculations of the properties.

Although improvement of the NCC potential is possible and under way, we believe that this potential can be applied to simulations of more complex systems as, for example, interphases and biomolecular solutions.

Acknowledgments: We wish to thank D. Estrin and V. Martorana for helpful discussions. This work has been carried out with the support of "Regione Autonoma Sardegna".

References

1. U. Niesar, G. Corongiu, E. Clementi, G.R. Kneller, and D. Bhattacharya, J. Phys. Chem. **94**, 7949 (1990).
2. G. Corongiu, Int. J. Quantum Chem. **44**, 1209 (1992).
3. G. Corongiu and E. Clementi, J. Chem. Phys. **97**,2030 (1992).
4. F. Sciortino and G. Corongiu J. Chem. Phys. 1992, Submitted.
5. R. Bartlett, I. Shavitt, and G.D. Purvuis, J. Chem. Phys. **71**, 281 (1979).
6. W. S. Benedict, N. Gailar, and E. K. Plyler, J. Phys. Chem. **24**, 1139 (1956).
7. (a) A. H. Narten and H. A. Levy, J. Chem. Phys. **55**, 2263 (1971); (b) L. Bosio, S.H. Chen and J. Teixeira, Phys. Rev. A **27**, 1468 (1983).
8. A. H. Narten, J. Chem. Phys. **56**, 5681 (1972).
9. A. K. Soper and M. G. Phillips, J. Chem. Phys. **107**, 47 (1986); A. K. Soper and R. N. Silver, Phys. Rev. Lett. **49**, 471 (1982).
10. The same property is found for the g_{OH} and g_{HH} functions. See Ref. 3.
11. S.H. Chen and J. Teixeira, J. Adv. Chem. Phys. **64**, 1 (1985).
12. F. Sciortino, A. Geiger and H. E. Stanley, Phys. Rev. Lett. **65**, 3452 (1990).
13. F. Sciortino, A. Geiger and H. E. Stanley, Nature **354**, 218 (1991).
14. F. Sciortino, A. Geiger and H. E. Stanley, J. Chem. Phys. **96**, 3857 (1990).
15. G. Corongiu and E. Clementi, in preparation.
16. G. E. Walrafen, M.S. Hokmabadi, and W.-H. Yang, J. Chem. Phys. **92**, 2433 (1988).
17. W.F. Kuhs and M.S. Lehmann in *Water Science Reviews*, Vol. 2 F. Franks Ed., University Press, Cambridge, 1986.
18. H.J. Prasak, S.F. Trevino, J.D. Gault and K.W. Logan, J. Chem. Phys. **56**, 3217 (1972).
19. B. Renker, in *Phonons*, edited by M.A. Nusimovici (Flammarion, Paris, 1971), p.167.
20. R.E. Gagnon, Kiefte and M.J. Clouter, J. Chem. Phys. **92**, 1909 (1990).
21. F. Sciortino and G. Corongiu, in preparation.
22. R. Frattini, M. Sampoli, M.A. Ricci and G. Ruocco, Chem. Phys. Letts **141**, 297 (1987); M.A. Ricci, G. Ruocco, M. Sampoli, Mol. Phys. **67** 19 (1989).
23. H. Popkie, H. Kistenmacher, and E. Clementi, J. Chem. Phys. **59**, 1325 (1973).
24. O. Matsuoka, E. Clementi and M. Yoshimine, J. Chem. Phys. **64**, 1351 (1976).